Article ID: 1000-324X(2023)07-0839-06 **DOI:** 10.15541/jim20220638

Correlation between Constitutive Behavior and Fracture Performance of PZT Ceramics

WANG Xueyao[1], WANG Wugang[2], LI Yingwei[1], PENG Qi[1], LIANG Ruihong[2]

(1. School of Civil Engineering, Wuhan University, Wuhan 430072, China; 2. Shanghai Institute of Ceramics, Chinese Academy of Sciences, Shanghai 200050, China)

Abstract: The fracture properties of ferroelectrics directly determine their processability and reliability of devices made of them. However, both experimentally and theoretically reported fracture toughness of piezoelectric ceramic materials remains nearly the same as that reported 30 years ago, limiting the application of piezoelectric devices in situation where high reliability is required. Here, we try to reveal the parameters that could be used to optimize the fracture performance of ferroelectrics. Specifically, stress-strain curves, intrinsic fracture toughness and long-crack fracture toughness of three typical PZT ceramics were measured by uniaxial compression method, crack-tip opening displacement (COD) technique and single-side V-notch beam (SEVNB) technique, respectively. It is shown that the intrinsic fracture toughness is positively correlated with the Young's modulus of the material, which suggests that improving the Young's modulus of ferroelectrics is an effective way to improve their intrinsic fracture toughness. The long-crack fracture toughness is related to the intrinsic toughness and extrinsic ferroelastic domain switching/phase transformation toughening, which also suggests that optimizing the ferroelastic switching behavior of piezoelectric ceramics can improve their extrinsic effect. Compared to the hard doped PZT, the soft doped PZT has low coercive stress, high remanent strain and high shielding toughness. The fracture patterns observed in different PZT materials are related to the different ferroelastic switching behavior of the materials. Soft PZT ceramics exhibit intergranular fracture, while hard PZT with weak ferroelastic switching behavior exhibits transgranular fracture. In conclusion, fracture toughness of ferroelectrics is enhanced by optimizing Young's modulus and toughening of ferroelastic switching.

Key words: lead titanate zirconate; crack-tip fracture toughness; ferroelastic domain switching; single-edge V-notch beam; fracture mode

Piezoelectric ceramics have been widely used in modern industries working as actuators, transducers, *etc*., due to their unique electromechanical coupling performance, ultra-fast response and small size[1-2]. After several decades of intensive investigations, the functional property of piezoelectric ceramic materials have been significantly improved, and some new piezoelectric ceramic systems were also developed[3-4]. In comparison, the mechanical property of piezoelectric ceramic materials, *e.g.*, fracture toughness and strength[5], are also very important, as the mechanical performance directly determines their processability, and the reliability of piezoelectric devices[6-7]. However, although tremendous investigations related to the fracture behavior of piezoelectric ceramic materials have been conducted by researchers in the last 30 years, both experimentally and theoretically[8-9], the reported fracture toughness K_{Ic} of piezoelectric ceramic materials remains near the same as that reported 30 years ago, in range of 0.5–1.1 MPa·m$^{1/2}$ for unpoled PZT ceramics[10-14]. To a certain extent, this situation has limited the application of piezoelectric devices in situation where high reliability is required.

At the moment, most of the fracture behaviors of piezoelectric ceramic materials observed in experiments or problems encountered in the industries could be well

Received date: 2022-10-31; **Revised date:** 2022-12-23; **Published online:** 2023-03-09
Foundation item: National Natural Science Foundation of China (11972262); Guangdong Provincial Key Laboratory Program (2021B1212040001)
Biography: WANG Xueyao (1996–), female, PhD candidate. E-mail: 2014301890049@whu.edu.cn
王雪瑶(1996–), 女, 博士研究生. E-mail: 2014301890049@whu.edu.cn
Corresponding author: LI Yingwei, associate professor. E-mail: yingweili@whu.edu.cn;
LIANG Ruihong, professor. E-mail: liangruihong@mail.sic.ac.cn
李应卫, 副教授. E-mail: yingweili@whu.edu.cn; 梁瑞虹, 研究员. E-mail: liangruihong@mail.sic.ac.cn

explained, *e.g.*, the crack length-dependent fracture toughness (R-curve)[15-16] and the fracture toughness anisotropy of the materials after texturing[10-11,17-18]. As reviewed by Schneider[17], Kuna[19], Webber[20], *et al*., only a small number of problems are not well explained yet, for instance, the strange fracture surface mode–some piezoelectric ceramic materials undergo intergranular fracture, while some are dominated by transgranular fracture[21], and the different fracture mode in terms of hard and soft PZT[22]. Therefore, the next step of investigation on the fracture behavior of piezoelectric ceramic materials should focuse on proposing ideas or schemes that could be used to optimize the fracture behavior of ferroelectric ceramic materials. However, different from metals and other ceramics such as alumina ceramics, revealing the parameters that have influence on the fracture behavior of ferroelectric ceramic materials is a difficult task. This is because, on the one hand, the measured fracture toughness of piezoelectric ceramic materials is technique dependeddifferent charactering techniques normally lead to different fracture toughness values[18,23-24]. On the other hand, piezoelectric ceramic materials with different ferroelastic domain switching behavior have different toughening performance[10,13,20].

Hence, to reveal the parameters that could be referred for designing piezoelectric ceramic materials with better reliability, the constitutive behavior and the fracture performance should be both characterized. Moreover, materials with different performance but similar compositions should be characterized in comparison, which we tried to accomplish here. In this work, three types of commercially available PZT ceramics (PZT-4, -5, and -8) with different ferroelastic domain switching behaviors were chosen as model materials. The stress-strain curves of ceramics were firstly characterized during a uniaxial compression process to determine the parameters that have influence on the fracture behavior of ceramics. Then the intrinsic fracture toughness (also known as crack- tip fracture toughness) of ceramics, K_{I0}, was determined by the crack opening displacement (COD) technique. The long-crack fracture toughness of ceramics was also measured by the single-edge V-notch beam (SEVNB) technique. The scanning electron microscopy (SEM) was used to characterize the fracture mode of the crack surface. Based on the measured data, the different fracture performances of the three types of ceramics were discussed in comparison, by combining the measured fracture toughness, the constitutive behavior, and the intrinsic fracture toughness of these materials.

1 Experimental

1.1 Material description

The material compositions of the used PZT-4, -5, and -8 are $Pb_{0.95}Sr_{0.05}(Sb_{0.33}Nb_{0.77})_{0.1}Zr_{0.45}Ti_{0.45}O_3$-1%Fe, $Pb_{0.98}Sr_{0.02}(Zn_{0.33}Nb_{0.77})_{0.1}Zr_{0.45}Ti_{0.45}O_3$, and $PbZr_{0.53}Ti_{0.47}O_3$-0.6%Fe (in mol). They were fabricated by a standard solid-state synthesis process (S1). Their grain size and density are tabulated in Table S1.

1.2 Stress-strain curve measurement

The testing setup for characterizing the stress-strain behavior of the materials during uniaxial compression can be found in our previously published work[11] and S2.

1.3 Fracture toughness testing

Fig. 1 reveals an optical microscope image of a V-notch. The long-crack fracture toughness K_{Ivnb} of the specimen was calculated by[23]:

$$K_{Ivnb}=\left[\frac{F(S_1-S_2)}{BW^{1.5}}\right]\left[\frac{3\alpha^{0.5}}{2(1-\alpha)^{1.5}}\right]Y^* \quad (1)$$

where, F is the fracture stress, S_1 is the outer span, S_2 is the inner span, B is the specimen thickness, W is the specimen depth and $\alpha=a/W$, a is the average V-notch depth, Y^* is a dimensionless correction factor based on the ratio of a/W. The details of the test setup and the geometric dimensions of samples can be found in S3.

1.4 COD measurement

The crack-tip opening displacement (COD) technique was used to characterize K_{I0}. If no additional transverse or conical cracks appear and the residual stress field relaxes due to residual stress after the Vickers indentation is performed, the crack remains open. The details of measurement and computation are shown in S4.

Due to the toughening effect of the ferroelectric domain, the measured values gradually become larger than the estimated values, and the successive data points vary from the fitted straight line (Fig. 2(a)).

In addition to the preceding computation method mentioned above, the crack-tip fracture toughness can also be obtained by Irwin fitting[25]. That is, only A_0 (the coefficient based on the ratio of a/b) is used. This approach has the advantage of not requiring half-diagonal

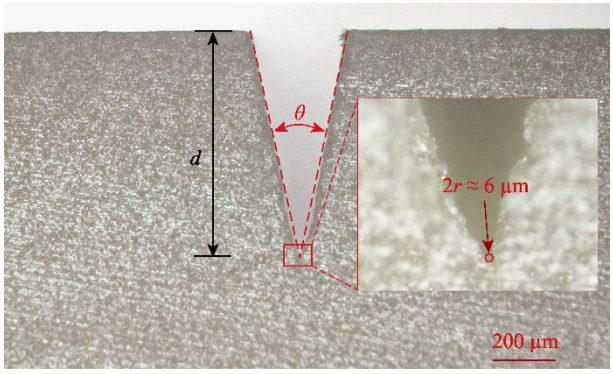

Fig. 1 Optical microscope image of a V-notch

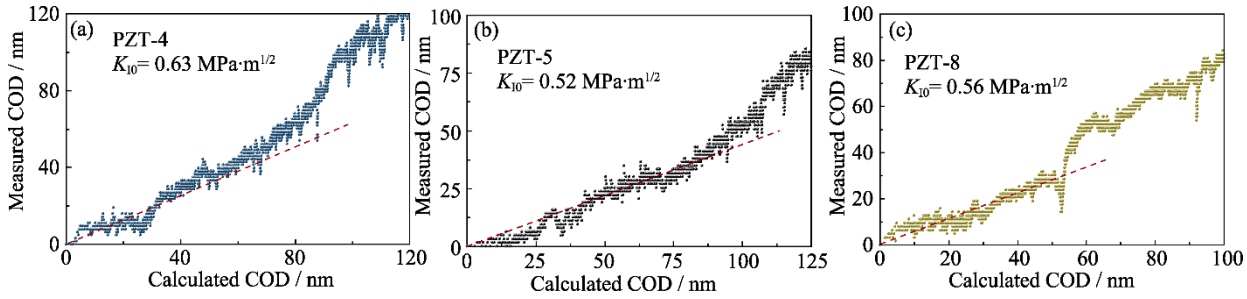

Fig. 2　Measured COD plotted *versus* the calculated COD
(a) PZT-4; (b) PZT-5; (c) PZT-8

length data for crack lengths and indentations. However, this evaluation is limited to the near-tip crack opening displacement field[25]. Fig. S1 shows the measured crack opening displacement COD as a function of the distance x from the crack tip and the least-squares fitting curves with x_{max}=10 μm.

2　Results and discussions

2.1　Stress-strain curves of the tested materials

Fig. 3 depicts the measured stress-strain curves during mechanical compression. At first, all of the materials reveal a linear stress-strain behavior, and then follow a significant nonlinear regime due to ferroelastic switching (in addition to non-180° ferroelastic domain switching, ferroelastic phase transformation can also induce nonlinear deformation for ferroelectrics, and both mechanisms can be called ferroelastic switching[26]), during which the strain accumulates quickly with the increase of the applied stress. With further increase of compressive stress, the stress-strain curves gradually change from nonlinearity to linearity, due to the decrease of the volume of domains that could be switched by the applied stresses. Additionally, based on the obtained stress-strain curves, the coercive stress σ_c, the remanent strain ε_r, the Young's modulus E and the Poisson's ratio ν of the tested materials can be determined and tabulated in Table S5.

2.2　Fracture toughness and fracture mode of the tested materials

Fig. 4 depicts the measured K_{Ivnb} and K_{I0} for unpoled PZT ceramics with different compositions. The K_{Ivnb} of PZT-5 is approximately 1.10 MPa·m$^{1/2}$, with a value similar to the results reported by others on PZT 151[10,27-29], *e.g.*, by Schneider with a value of 1.0 MPa·m$^{1/2}$[29]. In comparison, the K_{Ivnb} for PZT-4 is 0.91 MPa·m$^{1/2}$; for PZT-8, its K_{Ivnb} is 0.78 MPa·m$^{1/2}$. As for K_{I0}, the highest value is for PZT-4; the lowest value is for PZT-5; the intermediate value is for PZT-8. Additionally, for PZT-4, PZT-5 and PZT-8, the K_{I0} values determined by Eq. (S4-1)-Eq (S4-2) are 0.63, 0.52, and 0.56 MPa·m$^{1/2}$, respectively; which are slightly lower than the values of 0.75, 0.59, and 0.6 MPa·m$^{1/2}$ obtained *via* Irwin parabola. This is because A_1 (the coefficient based on the ratio of a/b) is positive for all the cracks evaluated in this work. Therefore, according to Eq. (S4-1), the K_{I0} for the same $u(x)$ is always higher if only A_0 is considered (Irwin parabola)[25]. Even the K_{I0} values determined by Irwin parabola could be higher than the observed K_{IC} value[30]. Thus, the three-term- approximation should be the first choice.

Fig. S2 displays the photography of the fracture surface characterized by SEM. For PZT-5, the fracture morphology is intergranular fracture dominated (~90%);

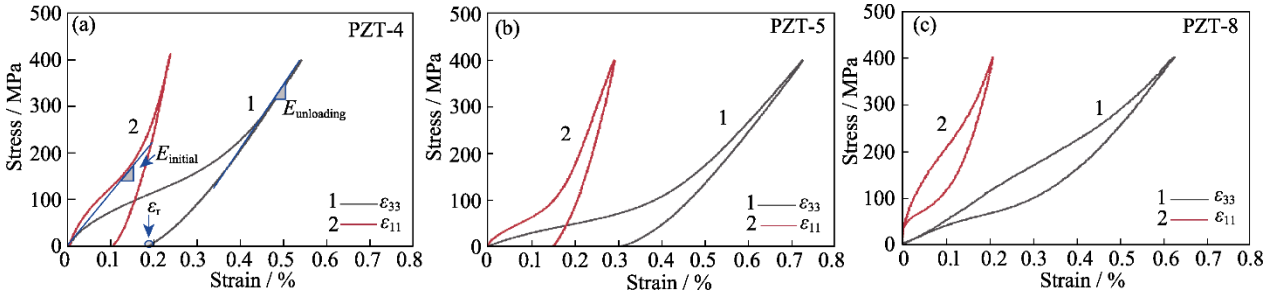

Fig. 3　Stress-strain curves of PZT obtained during mechanical compression
(a) PZT-4; (b) PZT-5; (c) PZT-8

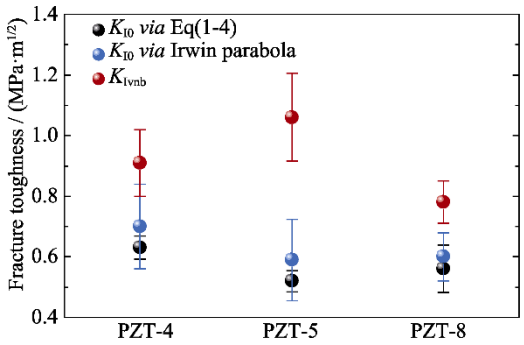

Fig. 4 Fracture toughness K_{Ivnb} and intrinsic fracture toughness K_{I0} for PZT-4, -5, and -8

while for PZT-4 and PZT-8, most parts of the fracture morphology are transgranular (~70% for PZT-4 and ~95% for PZT-8). It is in accordance with the previous reports of Guillon, *et al*[22]. They found that the fracture mode of PZT piezoceramics is related to the dopants, PZT with soft additives is mainly intergranular while PZT with hard additives is rather trangranular.

2.3 Discussions

As the intrinsic toughness is controlled by the atomic interactions of the materials, and is generally believed to be proportional to their theoretical tensile strength. Additionally, the theoretical tensile strength of a material is thought to be one tenth of its Young's modulus. For PZT-4, -5, and -8, 1 : 0.7 : 0.8 for both $E_{initial}$ and K_{I0}. This demonstrates that to improve the intrinsic fracture toughness of piezoelectric ceramics, we have to find strategy to improve their Young's modulus.

Additionally, from Fig. 4, it can be seen that the measured values of K_{Ivnb} and K_{I0} are controversial, *e.g.*, the largest K_{Ivnb} was observed in PZT-5, while it reveals the smallest K_{I0}. According to the previous investigations[23], such controversy can be rationalized by the toughening mechanism of ferroelastic switching. Under external load, stress concentrates near the crack tip with distributions dominated by the K_{appl}-stress field. Due to ferroelastic switching, this K_{appl}-stress field will trigger a process zone with dimensions related to the stress field distribution, the coercive stress σ_c, and the intrinsic toughness K_{I0} of the materials. For unpoled PZT ceramics, the domains with random orientations switch into the direction along the applied tensile stresses. This process zone, obviously, will shield the K_{appl}-stress field. With the growth of the crack, the process zone triggered by the K_{appl}-stress field becomes the crack wake. For PZT-4 and -5, the switched domain remained in the wake of crack, leading to the increase of the closure shielding stresses at the crack tip (Fig. 5(a)). To promote further increment of the crack, a larger applied stress is required. Therefore, under controlled load, the fracture toughness of piezoelectric ceramic materials normally reveals an R-curve behavior, and when the crack propagates a certain distance, a plateau value K_{IR}^{max} can be achieved. Obviously, the value K_{IR}^{max} is nearly equal to the sum of K_{I0} and K_{μ}^{max} (K_{IR}^{max} means the largest fracture toughness of ferroelectrics under controlled load; K_{μ}^{max} presents the maximum shielding toughness). That is $K_{IR}^{max} = K_{I0} + K_{\mu}^{max}$.

The calculated shielding toughness K_{μ}^{max} (S7) for PZT-4, -5, and -8 was 0.17, 0.24, and 0 MPa·m$^{1/2}$, respectively. Then the K_{IR}^{max} for PZT-4, -5, and -8 should be 0.80, 0.76, and 0.56 MPa·m$^{1/2}$, respectively, which are smaller than the test value of 0.91, 1.10, and 0.78 MPa·m$^{1/2}$. This phenomenon was possibly induced by other toughening mechanism that was not taken into consideration in Eq.(S7-1), for instance, the shielding effect of process zone near the crack tip, crack deflection toughening, the kink of the crack during propagation, and the crack-interface grain bridging. Taken PZT-8 as an example, the calculated K_{μ}^{max} is zero based on Eq. (S7-1) as the switched domains switch back in the crack wake (Fig. 5(b)). However, the measured K_{Ivnb} is larger than K_{I0}, with a value of 0.22 MPa·m$^{1/2}$.

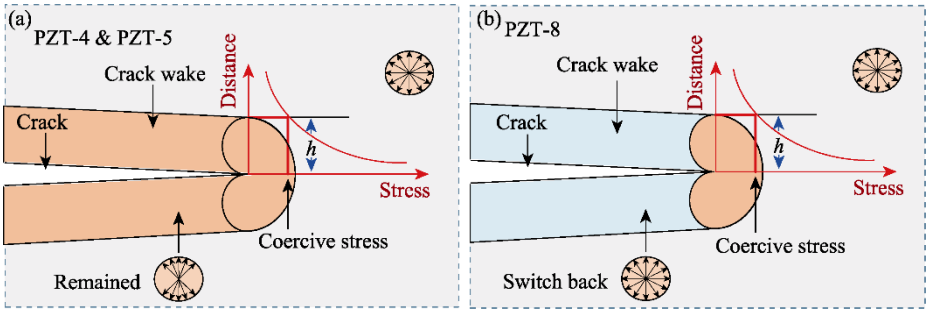

Fig. 5 Illustration of the toughening mechanism
(a) PZT-4 and PZT-5; (b) PZT-8

The difference between the observed intergranular and transgranular crack surfaces in different PZT is supposed to relate to the ferroelastic switching as well. In order to express our point of view more conveniently, it is firstly assumed that the tensile strength of the grain boundaries is weaker than the grains. Then for polycrystalline materials, if the grain boundaries are aligned with the crack growth path, the crack would propagate along with the grain boundary (Fig. S3(a)). However, in most cases, the grain interfaces are not parallel to the main crack, and hence, if the crack propagates along the grain interface, the crack tip is expected to experience mixed loading, and more energy is consumed (Fig. S3(b)). With the increase of the grain size, obviously, the influence of the crack kink on the stress redistribution increases. When the stress field near the crack tip increases to critical strength of the grains, the crack passes through the grains, leading to transgranular cracks. However, if the size of the grains is smaller than a critical value, the influence of the crack kink on the stress redistribution is limited. As a result, for materials with small grain size, the crack mode is normally intergranular dominated[21].

However, for PZT ceramics, apart from the crack kink, the ferroelastic switching can also influence the stress field within the few grains near the crack tip. As the ferroelastic switching in ferroelectrics is accomplished by domain nucleation and domain wall motion, and the existence of grain boundaries affects the continuity of the ferroelastic switching process, the stress on the grain interface could be enhanced or decreased, depending on the crystallographic direction of the grains near the crack tip[21]. For PZT-5, as its σ_c is significantly smaller than those of PZT-4 and PZT-8, these effects may dominate the fracture mode, leading to intergranular fracture. However, for PZT-4 and PZT-8, their σ_c is larger. Hence, the effect of ferroelastic domain switching on the stress redistribution at the grain interface is limited, and therefore, transgranular fracture is dominated in them. Guillon[22] suggested that soft additives may cause grain boundary segregation in soft PZT, which changed the grain boundary energy and weakened grain boundaries. To further understand the effect of domain inversion on crack propagation modes in ferroelectric materials, *in situ* experiments and phase field modeling are required.

3 Conclusions

In summary, by using three typical PZT ceramics as model materials, the correlation between their constitutive and fracture behavior was investigated. Their deformation behavior in the direction parallel or perpendicular to the applied stress were characterized under uniaxial compression at room temperature. Their fracture toughness was measured by SEVNB technique and K_{I0} was measured by COD technique, and the fracture mode was characterized by SEM. The different fracture performance of the three types of materials were discussed in comparison, by combining the measured fracture toughness, the constitutive behavior, and the intrinsic toughness of these types of materials. The main conclusions are as follows:

1) For PZT-4, -5, and -8, 1 : 0.7 : 0.8 for both E_{initial} and K_{I0}. This demonstrates that improving the Young's modulus of ferroelectrics is an effective way to improve their intrinsic fracture toughness.

2) The K_{Ivnb} of PZT-4, -5, and -8 are 0.91, 1.10, and 0.78 MPa·m$^{1/2}$, respectively. The controversy between K_{Ivnb} and K_{I0} revealed can be rationalized by the toughening mechanism of ferroelastic switching. These results demonstrate that by optimizing the ferroelastic switching behavior of piezoelectric ceramics, their extrinsic effect of $K_{\mu}^{\max}$ could be improved.

2) The difference between the observed intergranular and transgranular crack surfaces in different PZT is also related to the ferroelastic switching. Both the fracture mode and ferroelastic switching related to the grain size, so the fracture toughness of PZT ceramics with defined composition could be optimized by changing the grain size.

Supporting Materials

Supporting materials related to this article can be found at https://doi.org/10.15541/jim20220638.

References:

[1] AKSEL E, JONES J L. Advances in lead-free piezoelectric materials for sensors and actuators. *Sensors*, 2010, **10(3):** 1935.

[2] RODEL J, WEBBER K G, DITTMER R, *et al*. Transferring lead-free piezoelectric ceramics into application. *J. Eur. Ceram. Soc.*, 2015, **35(6):** 1659.

[3] DAMJANOVIC D. Ferroelectric, dielectric and piezoelectric properties of ferroelectric thin films and ceramics. *Rep. Prog. Physics*, 1998, **61(9):** 1267.

[4] RODEL J, LI F. Lead-free piezoceramics: status and perspectives. *MRS Bull*., 2018, **43(8):** 576.

[5] PISARENKO G, KOVALEV S P, CHUSHKO V M. Fracture toughness of piezoelectric ceramics. *Strength Mater*., 1980, **12(12):** 1492.

[6] RODIG T, SCHONECKER A, GERLACH G. A survey on piezoelectric ceramics for generator applications. *J. Am. Ceram. Soc.*, 2010, **93(4):** 901.

[7] GALLEGO-JUAREZ J A. Piezoelectric ceramics and ultrasonic transducers. *J. Phys. E Sci. Instrum.*, 1989, **22(22):** 804.

[8] PFERNER R A, THURN G, ALDINGER F. Mechanical properties of PZT ceramics with tailored microstructure. *Mater. Chem. Phys.*, 1999, **61(1):** 24.

[9] LI F X, FANG D N, SOH A K. Theoretical saturated domain-

orientation states in ferroelectric ceramics. *Scr. Mater*., 2006, **54(7):** 1241.
[10] CALDERON-MORENO J M, POPA M. Fracture Toughness Anisotropy by Indentation and SEVNB on Tetragonal PZT Polycrystals. 12th Meeting of the International Conference on the Strength of Materials (ICSMA 12), 2001, **319:** 692.
[11] LI Y W, LI F X. Large anisotropy of fracture toughness in mechanically poled/depoled ferroelectric ceramics. *Scr. Mater*., 2010, **62(5):** 313.
[12] CALDERON-MORENO J M, GUIU F, MEREDITH M, *et al*. Fracture toughness anisotropy of PZT. *Mater. Sci. Eng. A*, 1997, **234–236(1):** 1062.
[13] MEHTA K, VIRKAR A V. Fracture mechanisms in ferroelectric-ferroelastic lead zirconate titanate (Zr: Ti=0.54:0.46) ceramics. *J. Am. Ceram. Soc*., 1990, **73(3):** 567.
[14] LUCATO SLDE; LUPASCU DC; RODEL J. Effect of poling direction on R-curve behavior in lead zirconate titanate. *J. Am. Ceram. Soc*., 2000, **83(2):** 424.
[15] FETT T, GLAZOUNOV A, HOFFMANN M J, *et al.* On the interpretation of different *R*-curves for soft PZT. *Eng. Fract. Mech.*, 2001, **68(10):** 1207.
[16] SEO Y H, VOGLER M, ISAIA D, *et al*. Temperature-dependent *R*-curve behavior of $Pb(Zr_{1-x}Ti_x)O_3$. *Acta Mater*., 2013, **61(17):** 6418.
[17] SCHNEIDER G A. Influence of electric field and mechanical stresses on the fracture of ferroelectrics. *Annu. Rev. Mater. Res*., 2007, **37:** 491.
[18] LI Y W, LIU Y, OCHSNER P E, *et al*. Temperature dependent fracture toughness of KNN-based lead-free piezoelectric ceramics. *Acta Mater.*, 2019, **174:** 369.
[19] KUNA M. Fracture mechanics of piezoelectric materials-where are we right now? *Eng. Fract. Mech*., 2010, **77(2):** 309.
[20] WEBBER K G, VOGLER M, KHANSUR N H, *et al*. Review of the mechanical and fracture behavior of perovskite lead-free ferroelectrics for actuator applications. *Smart Mater. Struct.*, 2017, **26(6):** 063001.
[21] KIM S B, KIM D Y, KIM J J, *et al.* Effect of grain size and poling on the fracture mode of lead zirconate titanate ceramics. *J. Am. Ceram. Soc*., 1990, **73(1):** 161.
[22] GUILLON O, THIEBAUD F, PERREUX D, *et al.* New considerations about the fracture mode of PZT ceramics. *J. Am. Eur. Soc*., 2005, **25:** 2421.
[23] KUBLER J. Fracture toughness of ceramics using the SEVNB method a joint VAMSA/ESIS round robin. *Fract. Mech. Ceram*., 2002, **13:** 437.
[24] SALEM J A. Fracture toughness of advanced ceramics at room temperature. *J. Res. Natl. Inst. Stand. Technol.*, 1992, **97(5):** 579.
[25] VOGLER M, FETT T, RODEL J. Crack-tip toughness of lead-free $(1-x)(Na_{1/2}Bi_{1/2})TiO_3–xBaTiO_3$ piezoceramics. *J. Am. Ceram. Soc*., 2018, **101(12):** 5304.
[26] LI F X, SOH A K. An optimization-based computational model for domain evolution in polycrystalline ferroelastics. *Acta Mater.*, 2010, **58(6):** 2207.
[27] BERMEJO R, DELUCA M. Mechanical characterization of PZT ceramics for multilayer piezoelectric actuators. *J. Ceram. Sci. Technol*., 2012, **3(4):** 159.
[28] BERMEJO R, GRUNBICHLER H, KREITH J, *et al.* Fracture resistance of a doped PZT ceramic for multilayer piezoelectric actuators: Effect of mechanical load and temperature. *J. Eur. Ceram. Soc*., 2010, **30(3):** 705.
[29] JELITTO H, KEBLER H, SCHNEIDER G A, *et al*. Fracture behavior of poled piezoelectric PZT under mechanical and electrical loads. *J. Eur. Ceram. Soc*., 2005, **25(5):** 749.
[30] DENKHAUS S M, VOGLER M, NOVK N, *et al.* Short crack fracture toughness in $(1-x)(Na^{1/2}Bi^{1/2})TiO_3–xBaTiO_3$ relaxor ferroelectrics. *J. Am. Ceram. Soc*., 2017, **100(10):** 4760.

PZT 陶瓷本构行为与断裂性能的相关性研究

王雪瑶[1], 王武港[2], 李应卫[1], 彭 奇[1], 梁瑞虹[2]

(1. 武汉大学 土木建筑工程学院, 武汉 430072; 2. 中国科学院 上海硅酸盐研究所, 上海 200050)

摘 要: 铁电陶瓷的力学性能直接决定了其加工性能和铁电器件的可靠性。目前, 无论是实验还是理论报道的压电陶瓷材料的断裂韧性都与 30 年前的报道接近, 限制了压电器件在高可靠性要求的情况下的应用。本研究试图揭示可用于优化铁电陶瓷断裂性能的参数。利用单轴压缩方法、裂纹尖端张开位移(Crack-tip opening displacement, COD)技术和单边 V 型缺口梁(Single-side V-notch beam, SEVNB)技术分别测定三种典型 PZT 陶瓷的应力-应变曲线、本征断裂韧性和长裂纹断裂韧性。结果表明, 本征断裂韧性与材料的杨氏模量正相关, 说明提高铁电体的杨氏模量是提高其本征韧性的有效途径。长裂纹断裂韧性与本征韧性和非本征铁弹性畴变/相变增韧有关, 说明优化铁电陶瓷的铁弹翻转行为可以改善其非本征效应。软掺杂 PZT 相较于硬掺杂 PZT 具有较低的矫顽应力和较高的残余应变, 呈现较强的铁弹性翻转和较高的屏蔽韧性; 在不同 PZT 材料中观察到的断裂模式也被认为与材料不同的铁弹性翻转行为有关, 软 PZT 陶瓷呈现沿晶断裂, 铁弹性翻转较弱的硬 PZT 呈现穿晶断裂。综上所述, 优化铁电材料的杨氏模量和铁弹翻转行为有望提升其断裂韧性。

关 键 词: 锆钛酸铅; 裂纹尖端断裂韧性; 铁弹性畴翻转; 单边 V 型缺口梁; 断裂模式

中图分类号: TQ174 **文献标志码:** A

Supporting Materials:

Correlation between Constitutive Behavior and Fracture Performance of PZT Ceramics

WANG Xueyao[1], WANG Wugang[2], LI Yingwei[1], PENG Qi[1], LIANG Ruihong[2]

(1. School of Civil Engineering, Wuhan University, Wuhan 430072 Wuhan, China; 2. Shanghai Institute of Ceramics, Chinese Academy of Sciences, Shanghai 200050, China)

S1　Preparation of ceramics

The materials were fabricated by a standard solid-state synthesis process using high-purity powders as raw ingredients. The weighted powder was first processed for 4 h in a planetary ball mill, after which the slurry was taken out and dried, pressed into large pieces, and synthesized for 2 h at 850 ℃. The powder was then crushed and re-milled in a planetary ball mill with the appropriate amount of water for 6 h. After extraction and drying, PVA is added to the powder for granulation, which is then pressed into rectangular strips using a uniaxial press. The pressed sample was sintered at 1200–1300 ℃ for 2–3 h after being heated to 650 ℃ for 1 h to volatilize PVA.

Before testing, all samples were annealed at 450 ℃ for 1 h to release the residual stress induced during cutting. According to the SEVNB technique reported by Kübler[1], the used samples were machined into bar shape with dimensions of 3 mm×4 mm×27 mm. For each data point of the fracture toughness, at least five measurements were taken, then the average value and the standard deviation were calculated to ensure representative results. The dimension of the samples used to characterize the stress-strain curves is 4 mm×4 mm×10 mm.

Table S1 Microstructural properties of the investigated materials

Material	Density /(g·cm^{-3})	Grain size/μm
PZT-4	7.7	(2.5±0.5)
PZT-5	7.8	(5.0±0.5)
PZT-8	7.6	(2.5±0.5)

S2　Details of stress-strain test

The deformation in the direction along and perpendicular to the applied stress were both measured uring uniaxial compression. The compressive stress is applied to the specimens by a screw-driven testing machine, together with a spherical hinge to avoid any bias stress. Strains gauges are glued on the four 4 mm×10 mm surfaces of the specimens to measure the longitudinal and transversal deformation. The signals of the stress and strain are input into an A/D data acquisition card monitored by a computer. During testing, a preload of about 20 N was applied on the specimens firstly, and then the strain signals were checked, based on which the position of the specimens was adjusted to assure uniaxial compression without bending. The loading rate is set to be 1 MPa/s, and unloading starts with rate of 1 MPa/s when the applied load reaches 400 MPa.

S3　Details of fracture toughness test

The V-shaped notch was introduced at the center of the 3 mm×27 mm surfaces of the bar samples by a cutting machine provided by Wuhan Dislocation Technology Company. A servo motor guides the straight reciprocating motion of a razor blade. Diamond particles were pasted on the razor blade to aid the cutting speed, which intended to introduce a V-notch on the surface of the sample. The moving speed of the razor blade and the cutting depth of the V-shaped notch are both controlled automatically. In addition, the cutting machine can control and monitor the contact force between the blade and the sample. Under the contact force of about 1 N, the slow cutting speed can greatly avoid the damage to the notch. During operation, a V-shaped notch with a depth of ~1 mm was cut on the sample first, and then replaced the old blade by a new one to finish the cutting process. After cutting, no obvious damage was observed near the notch by optical microscope.

The geometric dimensions of the V-notch crack were characterized under optical microscope. The determined depth d, the radius of the V-notch root r, and the angle θ between the two surfaces vary from 0.89 mm to 1.18 mm, 3 μm to 8 μm, and 24° to 30°, respectively, satisfying the requirements of the SEVNB technique[S1]. The specimens were then fractured by four-point bending with an inner span of 10 mm and an outer span of 20 mm. During testing, the applied load increased monotonically at a rate

of 0.5 mm/min until the sample fractured. After fracture, crack surfaces were characterized by scanning electron microscopy (SEM).

For Eq. (1), Y^* is a dimensionless correction factor based on the ratio of a/W, which has the form:

$$Y^* = 1.9887 - 1.326\alpha - [(349 - 0.68\alpha + 135\alpha^2)\alpha(1-\alpha)/(1+\alpha)^2] \quad \text{(S3-1)}$$

S4 COD calculation

First, the surface of the sample containing the indentation is meticulously polished in a series of steps using 10–0.1 mm diamond paste and ultrasonically cleaned after polishing. The cracks were induced by Vickers indentation with applied load of 49 N for 10 s. The gold was then sputtered onto the same surfaces as the conductive layer. A magnification of 70000 times was taken with an SEM at the crack - tip region and 35000 times at sufficiently large crack opening displacement. The step size between the images were increased with increasing distance to the crack - tip and chosen magnification. Finally, the semi-automatic procedure method developed by Vögler[S2] was used to calculate the crack opening displacement u as a function of the crack tip distance x. For every image, the crack was selected via a gray threshold and divided into 70 equally large segments. For each segment, the average crack opening displacement was calculated[S2].

The crack opening displacement field can be characterized using the equation derived by Fett, *et al*[S3] for semi-elliptical cracks caused by Vickers indentation:

$$u = K_{I0}\frac{\sqrt{b}}{E'}\left[A_0\left(\frac{x}{b}\right)^{1/2} + A_1\left(\frac{x}{b}\right)^{3/2} + A_2(x/b)^{5/2} + \cdots + A_n(x/b)^{n+1/2}\right] \quad \text{(S4-1)}$$

where

$$A_0 = \sqrt{8/\pi} \quad \text{(S4-2(a))}$$

$$A_1 = 11.7\exp\left[-2.063\left(\frac{a}{b}-1\right)^{0.28}\right] - 0.898/\left(\frac{a}{b}-1\right) \quad \text{(S4-2(b))}$$

$$A_2 = 44.5\exp\left[-3.712\left(\frac{a}{b}-1\right)^{0.28}\right] - \frac{1}{(a/b-1)^{1/2}} \quad \text{(S4-2(c))}$$

and x represents the distance from the crack tip, a represents the length of the crack measured from the center of the indentation to the crack tip, b represents the half-diagonal length of the indentation, E' represents the effective Young's modulus of the material. It is sufficient to use the coefficients $A_0 - A_2$ for cracks between $1.4 < a/b < 3.5$ in the calculation. Because the crack lies in the plane of the strain, the effective Young's modulus is used[S3-S4]:

$$E' = E/(1-\nu^2) \quad \text{(S4-3)}$$

where ν is the Poisson's ratio.

Assuming K_{I0} = 1 MPa·m$^{1/2}$, and combining the measured a, b, Y', x, we may get the computed crack displacement u_{comp} by utilizing formulas (S4-1, 2), then plot together with the measured crack displacement u_{meas} results. And the actual crack-tip fracture toughness of the material can be derived from the slope of the fitted line through the origin dot, as illustrated by the red line in the Fig. 2.

Fig. S1 shows that the measured COD gradually deviates from the Irwin parabola fitting curve, which is mainly related to two reasons: (i) The nonlinearity of the materials will affect the crack-tip opening displacement; (ii) The crack-tip opening displacement is affected by the indentation residual stress field. However, it should be pointed out that since the ferroelastic switching has been completed at the near-tip (the region within 10 μm), the residual stress field caused by the indentation will not affect the opening displacement in this region (the opening displacement at the near-tip is controlled by the near-tip stress field). Therefore, only the region within 10 μm of the crack tip is selected for fitting.

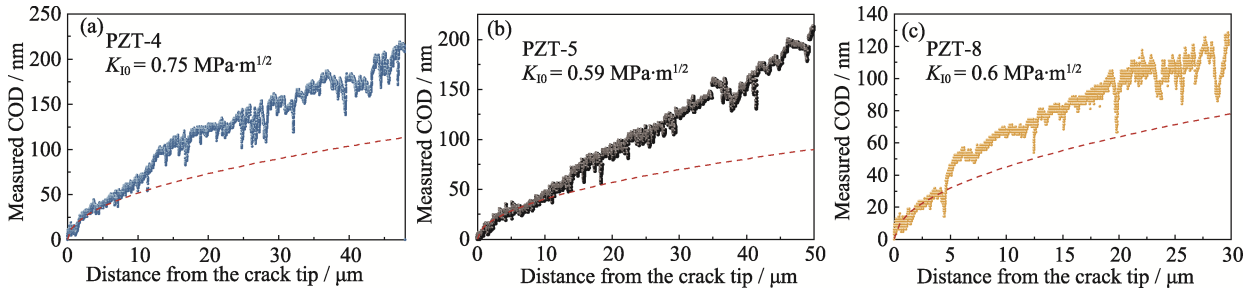

Fig. S1 COD profiles for (a) PZT-4, (b) PZT-5, and (c) PZT-8
The Irwin parabola is represented by the red line

S5　Mechanical properties of the investigated materials

By dividing the strain with stress, the loading part of the stress-strain curve can be replotted as $\mathrm{d}\varepsilon/\mathrm{d}\sigma$ as a function of the applied stress, and based on which, we can figure out an inflection point that is normally defined as coercive stress of σ_c [S5]. At σ_c, obviously, the materials present the maximum ferroelastic domain switching speed. For PZT-4, -5, and -8, the determined σ_c are ~120, ~55, ~170 MPa, respectively.

During unloading, the strain displays linear behavior first and then follows a nonlinear performance. For PZT-4 and -5, significantly remanent strain was observed (Fig. 3(a, b)). The smallest critical stress was observed for PZT-5, with values of ~25 MPa (Fig. 3(b)); the largest critical stress was observed for PZT-8, with values of ~125 MPa (Fig. 3(c)); intermediate critical stress of ~40 MPa was determined for PZT-4 (Fig. 3(a)). When the applied stresses reach 400 MPa, the measured longitudinal strain ε_{33} for PZT-4, -5, and -8 are 0.55%, 0.73%, and 0.64%, respectively. The measured strains at zero stress from the data of ε_{33} are normally defined as the remanent strain ε_r, which are 0.18% and 0.32% for PZT-4 and -5, respectively. However, for PZT-8, the plastic deformation observed during loading was completed recovered during unloading (Fig. 3(c)). That is, the measured ε_r is zero.

Additionally, based on the obtained stress-strain curves, the Young's modulus E and the Poisson's ratio ν of the tested materials can be determined. The Poisson's ratio ν is calculated from the ratio of transverse strain to longitudinal strain. The E recorded during initial loading (E_{initial}) represents the Young's modulus of the material in the unpoled state; the E determined during initial unloading from the maximum stress level ($E_{\mathrm{unloading}}$) represents the Young's modulus along the loading direction for the mechanically textured sample. Similarly, two different values of the Poisson's ratio can be determined. For the material in the unpoled state, the initial Poisson's ratio ν_{initial} for PZT-4, -5, and -8 are 0.4, 0.33, and 0.12, respectively; the Poisson's ratio determined during initial unloading from the maximum stress level ($\nu_{\mathrm{unloading}}$) are 0.35, 0.33 and 0.27 for the mechanically textured PZT-4, -5, and -8, respectively.

The determined values of coercive stress σ_c, the remanent strain ε_r, the Young's modulus E and the Poisson's ratio ν of the tested materials tabulated in Table S2.

S6　SEM micrographs of the fracture surfaces

It can be observed that the fracture surface morphology of the materials was consistent and without evolving during crack propagation from the micrograph characterized by SEM. Therefore, a representative fracture morphology micrograph was selected for each material.

S7　Proportionality factor

According to the previous investigations, the shielding fracture toughness $K_\mu^{\max}$ can be estimated by the following equation[S6]:

$$K_\mu^{\max}=\frac{0.22E\lambda\varepsilon_r\sqrt{1/2\pi}K_{I0}}{-0.22E\lambda\varepsilon_r\sqrt{1/2\pi}+(1-\nu)\sigma_c} \qquad \text{(S7-1)}$$

Here λ is the proportionality factor induced by the domain switching behavior difference under tensile and compressive stresses. Near room temperature, the tested material is composed of the rhombohedral (R) phase and the tetragonal (T) phase, and the fraction of the R phase and T phase are nearly equal, then λ is nearly equal to 1.41[S7]. The other parameters have been determined based on the stress-strain curves displayed above.

Table S2　Determined values of σ_c, ε_r, E_{initial}, $E_{\mathrm{unloading}}$, ν_{initial}, and $\nu_{\mathrm{unloading}}$

Material	σ_c/MPa	ε_r/%	E_{initial}/GPa	$E_{\mathrm{unloading}}$/GPa	ν_{initial}	$\nu_{\mathrm{unloading}}$
PZT-4	120	0.18	73	154	0.4	0.35
PZT-5	55	0.32	53	131	0.33	0.33
PZT-8	170	0	58	114	0.12	0.27

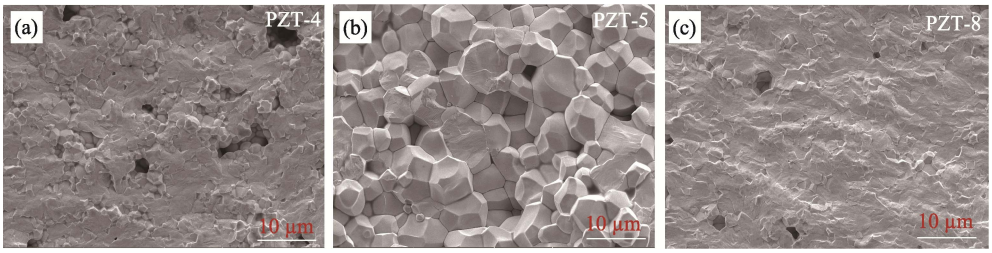

Fig. S2　SEM images of (a) PZT-4, (b) PZT-5 and (c) PZT-8

S8 Crack propagation

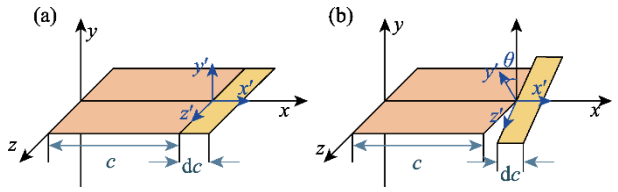

Fig. S3 Crack propagates along a grain boundary

(a) With direction parallel to the main crack; (b) With an angle of θ to the main crack

References:

[S1] KUBLER J. Fracture toughness of ceramics using the SEVNB method a joint VAMSA/ESIS round robin. *Fract. Mech. Ceram*., 2002, **13:** 437.

[S2] VOGLER M, FETT T, RODEL J. Crack-tip toughness of lead-free $(1-x)(Na_{1/2}Bi_{1/2})TiO_3$–$x$BaTiO$_3$ piezoceramics. *J. Am. Ceram. Soc*., 2018, **101(12):** 5304.

[S3] SCHNEIDER G A, FETT T. Computation of the stress intensity factor and COD for submicron sized indentation cracks. *J. Ceram. Soc. Japan*, 2006, **114(1335):** 1044.

[S4] FETT T, KOUNGA NJIWA A B, RODEL J. Crack opening displacements of Vickers indentation cracks. *Eng. Fract. Mech*., 2005, **72(5):** 647.

[S5] Zhou D, KAMLAH M, MUNZ D. Effects of bias electric fields on the non-linear ferroelastic behavior of soft lead zirconate titanate piezoceramics. *J. Am. Ceram. Soc.*, 2005, **88**: 867.

[S6] DENKHAUS S M, VOGLER M, NOVK N, *et al.* Short crack fracture toughness in $(1-x)(Na^{1/2}Bi^{1/2})TiO_3$–$x$BaTiO$_3$ relaxor ferroelectrics. *J. Am. Ceram. Soc*., 2017, **100(10):** 4760.

[S7] LI F X, FANG D N, SOH A K. Theoretical saturated domain- orientation states in ferroelectric ceramics. *Scr. Mater*., 2006, **54(7):** 1241.